J. Fluid Mech. (1998), *vol.* 367, *pp.* 205–220. Printed in the United Kingdom

Numerical simulation of superoscillations of a Triton-bearing drop in microgravity

By XIAOHUI CHEN[1], TAO SHI[2], YUREN TIAN[1], JOESEPH JANKOVSKY[1], R. GLYNN HOLT[3] AND ROBERT E. APFEL[1]

[1] Department of Mechanical Engineering, Yale University, New Haven, CT 06520-8286, USA

[2] Department of Radiology, Thomas Jefferson University, Philadelphia, PA 19107, USA

[3] Department of Aerospace and Mechanical Engineering, Boston University, Boston, MA 02215, USA

(Received 6 March 1997 and in revised form 13 February 1998)

Large-amplitude nonlinear oscillations of an axially symmetric water drop of volume 7.33 cm^3, initial aspect ratio 3.4, with surfactant Triton X-100 of 1.4×10^{-4} g ml^{-1} (1 CMC), in microgravity are compared with predictions of the boundary-integral method. The small shear viscosity of the bulk phase, as well as the surface dilatational viscosity and surface shear viscosity are considered. When a very specific set of material properties is assumed, numerical simulations of the drop oscillations are in good agreement with the experimental results of drop oscillations measured in space during the second United States Microgravity Laboratory, USML-2. The obtained surface viscosities are in rough agreement with literature values.

1. Introduction

Space shuttle observations (Apfel *et al.* 1997; Holt *et al.* 1997) of large-amplitude oscillations of an axially symmetric water drop with the surfactant Triton X-100 have illustrated dramatic nonlinear excursions. We have numerically simulated such drop oscillations so that the surface properties associated with the presence of surfactant can be extracted.

It is well known that when a drop is positioned in air in microgravity, the surface tension will make the drop attain a minimum surface area so as to reach a state of minimum surface energy. When a surfactant is introduced in the drop and accumulates at the surface, the magnitude of the surface tension stress generally diminishes significantly. In general, surfactants affect drop oscillations in two distinct ways. The first is called the Marangoni effect: because of the local rates of area change (surface dilatation) caused by surface deformations, the inhomogeneous redistribution of surfactant leads to tension gradients along the surface (Marangoni 1871; Sternling & Scriven 1959; Scriven 1960; Scriven & Sternling 1964). As the drop oscillates, the surfactant will diffuse between the bulk and the sublayer, and will adsorb and desorb between the sublayer and the surface. The surface tension gradients are governed by the bulk diffusion rate and the sorption rate. On the other hand, gradients exert a tangential force on the surface, and change the local value of the capillary pressure. To describe the Marangoni effect, the bulk diffusion coefficient and the sorption rates need to be known.

The second way oscillations are affected is due to the surface viscous stress caused

by the accumulation of surfactants at the surface. As the drop oscillates, there are surface shear flows and surface dilatational flows due to the local area expansion. The surfactants on the surface create a shear stress to resist the shear flow, and a surface normal stress to resist the surface dilatational flow. Related to the two surface stresses, there exist two surface viscosities: the surface shear viscosity and the surface dilatational viscosity (Scriven 1960; Scriven & Sternling 1964; Boussinesq 1913). They will contribute to the dissipation of energy, thereby increasing the damping rate of the drop oscillation over that caused by the shear viscosity of the bulk phase.

To simulate the oscillations of a drop with surfactants, we need to consider, in addition to the shear viscosity of the bulk phase, the Marangoni effect and the two surface viscosities. With so many unknown parameters, the theoretical analysis of the drop oscillation becomes complex. In the case presented here, special conditions make the theoretical analysis and numerical simulation tractable. First, the concentration of the surfactant in the bulk phase is sufficiently low that the bulk properties of the fluid, such as density and shear viscosity of the bulk phase, do not change. The fluid is assumed to be Newtonian. Second, the surface fluid is assumed to be of the Boussinesq type, so that the surface viscous stresses are linear functions of the rate of the surface strains with two proportionality constants: surface dilatational viscosity and surface shear viscosity. Third, surfactant diffusion from the bulk to the sublayer and sorption between the sublayer and the surface are fast enough so that the surface surfactant concentration as well as surface tension remain sensibly constant and homogenous when the drop oscillates. Therefore, we can ignore the 'Marangoni effect' caused by surface tension gradients for this particular case, although it is incorporated in the modelling for future consideration of other cases in which gradient effects are significant.

Lamb (1932, §349) shows that the small shear viscosity of the bulk phase produces a thin weak vortical layer at the free surface resulting in viscous damping of deep water waves. Lamb (1932) and Batchelor (1967) point out that dissipation is mainly in the irrotational part of the flow, not in the vortical layer. With the assumptions of a very thin vortical layer and low shear viscosity of the bulk phase, Lundgren & Mansour (1988) and Shi & Apfel (1995) have employed the boundary-integral method to study the nonlinear oscillations of large, axially symmetric liquid drops for the case of zero gravity and small shear viscosity of the bulk phase.

In this paper, we deal with a special case: oscillations of a drop with the surfactant Triton X-100, which is a polyethoxyether and is soluble in water. Its structure is $C_8H_{17} - (C_6H_4) - (OCH_2CH_2)_n - OH$, with n either 9 or 10. The assumption of constant surface tension for this particular case (Stebe 1989; Lin, McKeigue & Maldarelli 1990) is justified as follows.

It is well known that the transport of soluble surfactant is diffusion controlled. In the present case the concentration of Triton is 1.4×10^{-4} g cm^{-3} (1 CMC). Therefore, micelles are present in the solution. Van Hunsel, Bleys & Joos (1986) have studied the demicellization rate for Triton X-100 and have shown that it is larger than 10^2 s^{-1}. By fitting the contours of the experimental images, the maximum area dilatation rate of the surface of the drop, $1/A(\mathrm{d}A/\mathrm{d}t)$, is found to be less than 4.0 s^{-1}. Here A is the surface area. The surface area dilatation rate is much less than the demicellization rate. As described by Lin *et al.* (1990), micelles provide a reservoir for Triton to maintain a uniform sublayer concentration near the interface. Therefore, we can ignore the surfactant diffusion from the bulk to the sublayer of the surface as the drop oscillates. We only need to consider the kinetics between the sublayer and the surface.

When the surface Triton concentration reaches the value Γ_c, which corresponds to 1 CMC bulk Triton concentration, the surface tension is saturated and remains at approximately 33 dyne cm^{-1} (Stebe 1989; Lin *et al.* 1990; Apfel *et al.* 1997). Here Γ is the surface Triton concentration. As the drop surface area decreases, the corresponding surface surfactant concentration increases. If it is larger than Γ_c, the surface tension remains constant. Therefore, we need not consider the desorption rate in our case. We only need to consider the adsorption rate when the surface Triton concentration is lower than Γ_c.

While the surface area dilates, the surface Triton concentration decreases. If the adsorption rate is faster than the area dilatation rate as the drop oscillates, we can assume that the surface tension remains a constant throughout the drop oscillation. We evaluate the adsorption rate by calculating the time, t_0, in which the fresh surface reaches the 90% of the saturated surface Triton concentration Γ_c as the bulk Triton concentration remains 1 CMC. We use the Langmuir model:

$$\frac{d\Gamma}{dt} = \beta C_s(\Gamma_\infty - \Gamma) - \alpha\Gamma. \tag{1}$$

Here β and α are the factors for adsorption and desorption respectively, Γ_∞ is the saturated surface surfactant concentration, and C_s is the surfactant concentration in the sublayer. The adsorption rate is proportional to the concentration of surfactant C_s and the fraction of surface area unoccupied, while the desorption rate is proportional to the fraction of the area covered by adsorbed surfactant. Solving the above equation, we can derive the following result:

$$\Gamma = \frac{\beta C_s \Gamma_\infty}{\beta C_s + \alpha}(1 - e^{-(\beta C_s + \alpha)t}). \tag{2}$$

According to Stebe (1989) and Lin *et al.* (1990), β is larger than 10^8 cm^3 mol^{-1} s^{-1}, α is of the order 10^{-2} s^{-1}, and C_s approximates the bulk concentration, 3×10^{-7} mol cm^{-3}. Substituting these values into equation (2), we get $t_0 = 0.077$ s. In our case one cycle of oscillation T is about 0.83 s. Comparing t_0 to T, we can see that Triton adsorption is fast enough to maintain the surface surfactant saturation throughout the drop oscillation.

According to the above analysis, in considering the dynamics of a drop with Triton, only two variables are added to the surface stress: surface dilatational viscosity and surface shear viscosity. With small shear viscosity of the bulk phase (large Reynolds number) and small surface viscosities, we still can assume that the dissipation is mainly in the irrotational part of the flow both in the bulk and at the surface. This allows us to take advantage of the boundary-element method to simulate numerically this drop oscillation. The ultimate test of the approach is its ability to predict the observed behaviour.

2. Theory

Consider a water drop with surfactant statically positioned in air at negligible gravity. Because of an acoustic radiation force on it, the drop is deformed. When the acoustic force is suddenly decreased, free oscillations commence. The oscillation decays over time, which is numerically simulated based on the following formalism.

Consider an incompressible liquid with a free surface which separates it from air. The fluid in the drop satisfies the mass conservation equation and the Navier–Stokes

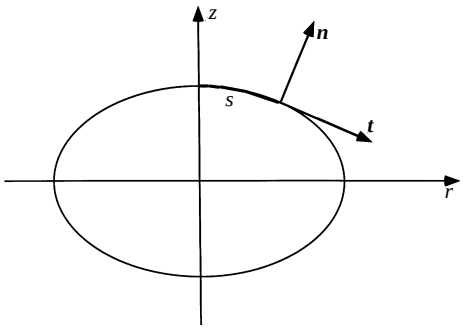

FIGURE 1. The coordinate systems for an axially symmetric drop

equations,

$$\nabla \cdot \boldsymbol{V}^* = 0, \tag{3}$$

$$\frac{\partial \boldsymbol{V}^*}{\partial t^*} + \boldsymbol{V}^* \cdot \nabla \boldsymbol{V}^* = -\frac{1}{\rho}\nabla P^* + \frac{\mu}{\rho}\nabla^2 \boldsymbol{V}^*. \tag{4}$$

Because the concentration of the surfactant in the liquid is sufficiently low, the bulk properties of the drop are assumed to be the same as those of water. Here, ρ is the water density, μ is the shear viscosity of the bulk phase of water, P^* is the pressure in the drop, $\boldsymbol{V}^*$ is the oscillation velocity vector, and * means the dimensional value. The coordinate system for this problem is shown in figure 1.

At the surface, there is a thin layer of surfactant. It must satisfy the surface momentum equation (Edwards, Brenner & Wasan 1991),

$$\rho^s \frac{\mathrm{d}_s \boldsymbol{V}^{s*}}{\mathrm{d}t^*} - \nabla_s \cdot \boldsymbol{P}^{s*} - \boldsymbol{F}^{s*} = \hat{\boldsymbol{n}} \cdot \parallel \overline{\boldsymbol{P}^*} \parallel . \tag{5}$$

Here $\boldsymbol{P}^{s*}$ is the second-order surface-excess pressure tensor, $\boldsymbol{F}^{s*}$ is the surface-excess force density vector, $\hat{\boldsymbol{n}} \cdot \parallel \overline{\boldsymbol{P}^*} \parallel$ is the difference between the force density vectors inside and outside the drop, $\hat{\boldsymbol{n}}$ is the unit normal direction vector at the drop surface, $\boldsymbol{V}^{s*}$ is the mass-averaged velocity vector of the surface, ρ^s is the surface-excess mass density and ∇_s is the surface gradient:

$$\nabla_s = \boldsymbol{I}_s \cdot \nabla. \tag{6}$$

$$\boldsymbol{I}_s = (\boldsymbol{I} - \hat{\boldsymbol{n}}\hat{\boldsymbol{n}}), \tag{7}$$

$$\frac{\mathrm{d}_s \boldsymbol{V}^{s*}}{\mathrm{d}t^*} = \frac{\partial \boldsymbol{V}^{s*}}{\partial t^*} + \boldsymbol{V}^{s*} \cdot \nabla \boldsymbol{V}^{s*}. \tag{8}$$

Owing to the extreme thinness of the surface transition zone, in all practical circumstances,

$$\rho^s = 0, \tag{9}$$

whence equation(5) reduces to the following boundary condition form:

$$-\hat{\boldsymbol{n}} \cdot \parallel \overline{\boldsymbol{P}^*} \parallel = \nabla_s \cdot \boldsymbol{P}^{s*} + \boldsymbol{F}^{s*}. \tag{10}$$

Boundary conditions

For axially symmetric flow, the velocity $\boldsymbol{V}^*$ lies in a meridian plane. Therefore, the boundary conditions at the free surface can be expressed as follows. The total stress

acting on the surface consists of three parts (Lu & Apfel 1991): pressure stress, bulk viscous stress and surface tension and viscous stress.

The pressure stress is

$$-\hat{\boldsymbol{n}}\cdot \parallel \overline{\boldsymbol{P}^*} \parallel_p = \hat{\boldsymbol{n}}P^*, \tag{11}$$

where P^* is the pressure in the drop.

The bulk viscous stress is

$$-\hat{\boldsymbol{n}}\cdot \parallel \overline{\boldsymbol{P}^*} \parallel_{bv} = -\hat{\boldsymbol{n}}\cdot 2\mu\boldsymbol{D}^*\cdot\hat{\boldsymbol{n}}\hat{\boldsymbol{n}} + \hat{\boldsymbol{n}}\cdot 2\mu\boldsymbol{D}^*\cdot\hat{\boldsymbol{t}}\hat{\boldsymbol{t}}, \tag{12}$$

where $\hat{\boldsymbol{t}}$ is the unit tangential vector at the surface as figure 1, and $\boldsymbol{D}^*$ is the second-order strain tensor:

$$\boldsymbol{D}^* = \tfrac{1}{2}(\nabla \boldsymbol{V}^* + \nabla \boldsymbol{V}^{*T}). \tag{13}$$

Also, the surface tension and viscous stress (Edwards *et al.* 1991) are

$$\begin{aligned}\nabla_s\cdot\boldsymbol{P}^{s*} = {} & -\hat{\boldsymbol{n}}(2H\sigma^*) - \hat{\boldsymbol{n}}[2\mu^s(\boldsymbol{b}-2H\boldsymbol{I}_s):\nabla_s\boldsymbol{V}^{s*} + 2H(k^s+\mu^s)\nabla_s\cdot\boldsymbol{V}^{s*}]\\ & +(k^s+\mu^s)\nabla_s\nabla_s\cdot\boldsymbol{V}^{s*} + \mu^s\{\hat{\boldsymbol{n}}\times\nabla_s[(\nabla_s\times\boldsymbol{V}^{s*})\cdot\hat{\boldsymbol{n}}]\\ & -2(\boldsymbol{b}-2H\boldsymbol{I}_s)\cdot(\nabla_s\boldsymbol{V}^{s*})\cdot\hat{\boldsymbol{n}}\},\end{aligned} \tag{14}$$

where σ^* is the surface tension coefficient, $2H$ is the mean surface curvature,

$$2H = -\nabla_s\cdot\hat{\boldsymbol{n}}, \tag{15}$$

μ^s is the surface shear viscosity and k^s is the surface dilatational viscosity owing to the presence of surfactants. In equation (14), $\boldsymbol{b}$ is a second-order tensor:

$$\boldsymbol{b} = -\nabla_s\hat{\boldsymbol{n}}. \tag{16}$$

Substituting equations (11), (12) and (14) into equation(10), we get the boundary conditions:

shear stress boundary condition

$$\begin{aligned}-\hat{\boldsymbol{n}}\cdot 2\mu\boldsymbol{D}^*\cdot\hat{\boldsymbol{t}}\hat{\boldsymbol{t}} + (k^s+\mu^s)\nabla_s\nabla_s\cdot\boldsymbol{V}^{s*} + \mu^s\{\hat{\boldsymbol{n}}\times\nabla_s[(\nabla_s\times\boldsymbol{V}^{s*})\cdot\hat{\boldsymbol{n}}]\\ -2(\boldsymbol{b}-2H\boldsymbol{I}_s)\cdot(\nabla_s\boldsymbol{V}^{s*}\cdot\hat{\boldsymbol{n}})\} = 0;\end{aligned} \tag{17}$$

normal stress boundary condition:

$$P^* + 2H\sigma^* = \hat{\boldsymbol{n}}\cdot 2\mu\boldsymbol{D}^*\cdot\hat{\boldsymbol{n}} - 2\mu^s(\boldsymbol{b}-2H\boldsymbol{I}_s):\nabla_s\boldsymbol{V}^{s*} - 2H(k^s+\mu^s)\nabla_s\cdot\boldsymbol{V}^{s*}. \tag{18}$$

3. Non-dimensionalization

The equations are put in dimensionless form by using parameters length a_0, velocity v_0 and time a_0/v_0. The length a_0 is taken as the radius of the spherical drop with equivalent volume as the non-spherical drop. P^* is replaced by the dimensionless term $P^*/(2\sigma/a_0)$. Assuming $2\sigma = \rho a_0 v_0^2$, we have

$$v_0 = [2\sigma/(\rho a_0)]^{1/2}. \tag{19}$$

Based on this v_0, the capillary wave velocity along the drop surface, a Reynolds number Re is calculated.

Thus, equations (3), (4), (17) and equation (18) are non-dimensionalized as follows:

governing equations

$$\nabla\cdot\boldsymbol{V} = 0, \tag{20}$$

$$\frac{\partial\boldsymbol{V}}{\partial t} + \boldsymbol{V}\cdot\nabla\boldsymbol{V} = -\nabla P + Re^{-1}\nabla^2\boldsymbol{V}; \tag{21}$$

boundary conditions

$$-\hat{\boldsymbol{n}} \cdot 2Re^{-1}\boldsymbol{D} \cdot \hat{\boldsymbol{t}}\hat{\boldsymbol{t}} + (K_e^{-1} + U_e^{-1})\nabla_s\nabla_s \cdot \boldsymbol{V}^s + U_e^{-1}\{\hat{\boldsymbol{n}} \times \nabla_s[(\nabla_s \times \boldsymbol{V}^s) \cdot \hat{\boldsymbol{n}}] - 2(\boldsymbol{b} - 2H\boldsymbol{I}_s) \cdot (\nabla_s \boldsymbol{V}^s \cdot \hat{\boldsymbol{n}})\} = 0, \tag{22}$$

$$P + H = \hat{\boldsymbol{n}} \cdot 2Re^{-1}\boldsymbol{D} \cdot \hat{\boldsymbol{n}} - 2U_e^{-1}(\boldsymbol{b} - 2H\boldsymbol{I}_s) : \nabla_s \boldsymbol{V}^s - 2H(K_e^{-1} + U_e^{-1})\nabla_s \cdot \boldsymbol{V}^s. \tag{23}$$

Here $Re \equiv \rho v_0 a_0/\mu$, $K_e \equiv \rho v_0 a_0^2/k^s$, and $U_e \equiv \rho v_0 a_0^2/\mu^s$, where K_e and U_e are the surface viscosity constants.

4. Solution procedures

Lundgren & Mansour (1988) point out 'For the viscous drop, the irrotational shear stress is not zero at the free surface. This small irrotational shear stress drags a thin viscous layer of rotational fluid along, making the small modification to the velocity field that is required in order to satisfy the zero-shear-stress boundary condition. This vortical layer is thin. The flow remains irrotational throughout the bulk of the fluid'. With this assumption and the fact that a liquid drop is axially symmetric, the problem is reduced to one dimension, and the calculation only requires information on the intersection of a meridian plane with the drop as in figure 1. Based on these theoretical considerations, Lundgren & Mansour (1988) study large Reynolds number drop oscillations with the boundary-integral method. In the present work, we incorporated surface viscous properties into the analysis. Because of the low concentration of the surfactant in the drop, we assume that the fluid properties of the bulk phase do not change. By fitting the contours of the experimental images, we determine a damping coefficient of approximately 0.07 s^{-1} in the oscillations of this Triton-bearing water drop with equivalent spherical diameter 2.41 cm. In the space shuttle, we also performed experiments on the oscillation of a pure water drop. With the same fitting analysis, we derived the damping coefficient of the oscillations of the pure water drop with equivalent spherical diameter 2.5 cm to be around 0.06 s^{-1}. This experimental comparison confirms the assumption that the surface viscosities of Triton are small; the Reynolds number Re and the surface viscosity constant K_e are of the same order, and the rotational velocity $U_t \propto O(\delta)$, here $\delta = Re^{-1/2}$. As in Lundgren's model (Lundgren & Mansour 1988), U_t is ignored in this paper. All of these assumptions afford us the opportunity to use Lundgren's method. With second-order $O(\delta^2)$ approximation and after performing the azimuthal integration, we get the following equations:

$$u_n = \boldsymbol{u} \cdot \hat{\boldsymbol{n}} = r^{-1}\frac{\partial r A_\theta}{\partial s}, \tag{24}$$

$$u_t = \boldsymbol{u} \cdot \hat{\boldsymbol{t}} = \frac{\partial \phi}{\partial s}, \tag{25}$$

$$\phi = \mu(\boldsymbol{r}) + \int_s [\mu(\boldsymbol{r}') - \mu(\boldsymbol{r})]K_\phi(\boldsymbol{r}, \boldsymbol{r}')\mathrm{d}s', \tag{26}$$

$$K_\phi = -\frac{r'}{\pi L}\left\{\frac{\hat{\boldsymbol{n}}' \cdot \boldsymbol{e}_r'}{2r'}[E(m) - K(m)] + \frac{\hat{\boldsymbol{n}}' \cdot (\boldsymbol{r} - \boldsymbol{r}')}{h^2}E(m)\right\}, \tag{27}$$

$$A_\theta = -\int_s [\mu(\boldsymbol{r}') - \mu(\boldsymbol{r})]K_A(\boldsymbol{r}, \boldsymbol{r}')\mathrm{d}s', \tag{28}$$

$$K_A = \frac{r'}{\pi L}\left\{\frac{\hat{\boldsymbol{t}}' \cdot \boldsymbol{e}_r'}{2r'}[E(m)-K(m)] + \frac{\hat{\boldsymbol{t}}' \cdot (\boldsymbol{r}-\boldsymbol{r}')}{h^2}\left[\frac{h^2}{2rr'}(K(m)-E(m))-E(m)\right]\right\}, \quad (29)$$

$$\frac{\mathrm{d}\boldsymbol{r}}{\mathrm{d}t} = \boldsymbol{u} + U_n \boldsymbol{e}_n, \quad (30)$$

$$U_n = \frac{1}{r}\frac{\partial r B_2}{\partial s}, \quad (31)$$

$$\frac{\mathrm{d}B_2}{\mathrm{d}t} = -(2\hat{\boldsymbol{t}} \cdot \nabla\boldsymbol{u} \cdot \hat{\boldsymbol{t}} + \boldsymbol{u} \cdot \hat{\boldsymbol{r}}/r)B_2 + 2R_e^{-1}\hat{\boldsymbol{n}} \cdot \nabla\boldsymbol{u} \cdot \hat{\boldsymbol{t}} - \{(K_e^{-1}+U_e^{-1})\nabla_s\nabla_s \cdot \boldsymbol{u}^s + U_e^{-1}\{\hat{\boldsymbol{n}} \times \nabla_s[(\nabla_s \times \boldsymbol{u}^s) \cdot \hat{\boldsymbol{n}}] - 2(\boldsymbol{b}-2H\boldsymbol{I}_s) \cdot (\nabla_s \boldsymbol{u}^s \cdot \hat{\boldsymbol{n}})\}\} \cdot \hat{\boldsymbol{t}}, \quad (32)$$

$$\frac{\mathrm{d}\phi}{\mathrm{d}t} = \frac{\boldsymbol{u} \cdot \boldsymbol{u}}{2} + U_n U_n + 2B_2 \hat{\boldsymbol{t}} \cdot \nabla\boldsymbol{u} \cdot \hat{\boldsymbol{n}} + 2Re^{-1}(\hat{\boldsymbol{t}} \cdot \nabla\boldsymbol{u} \cdot \hat{\boldsymbol{t}} + \boldsymbol{u} \cdot \hat{\boldsymbol{r}}/r) + H + 2U_e^{-1}(\boldsymbol{b}-2H\boldsymbol{I}_s) : \nabla_s \boldsymbol{u}^s + 2H(K_e^{-1}+U_e^{-1})\nabla_s \cdot \boldsymbol{V}^s, \quad (33)$$

$$L^2 = (z-z')^2 + (r+r')^2, \quad h^2 = (z-z')^2 + (r-r')^2, \quad m^2 = 1 - \frac{h^2}{L^2} = \frac{4rr'}{L^2}, \quad (34)$$

where $\boldsymbol{u}$ is the irrotational part of the velocity, and $\boldsymbol{U}$ is the rotational part of the velocity, so that $\boldsymbol{V} = \boldsymbol{u} + \boldsymbol{U}$. Here U_n and u_n are the normal rotational and irrotational velocities respectively; u_t is the irrotational tangential velocity; ϕ is the irrotational velocity potential, and $\boldsymbol{u} = \nabla\phi$. B_2 is the rotational vector velocity potential, $\boldsymbol{U} = \nabla \times B_2 \boldsymbol{e}_\theta$; $\boldsymbol{e}_r$, $\boldsymbol{e}_\theta$ and $\boldsymbol{e}_z$ form the cylindrical coordinates; r, z are the coordinates at the surface as in figure 1. Here s is the arclength from the top of the drop, and $\mu(\boldsymbol{r})$ is the dipole density. $E(m)$ and $K(m)$ are the first and second elliptic integrals which were computed using the accurate approximation formulae given in Abramowitz & Stegun (1972).

Given initial conditions, we can use equations (24)–(34) to simulate numerically the drop oscillation. The procedure for using the program is as follows: Before the drop is released, the deformed drop is statically positioned in the air for a period of time so that Triton reaches an equilibrium state. The initial scalar velocity potential ϕ, the vector rotational velocity potential B_2, and the initial positions r and z on the surface are known. With the end-point corrected trapezoidal quadrature method (Alpert 1990), from (26) the dipole density $\mu(\boldsymbol{r})$ is calculated. Substituting $\mu(\boldsymbol{r})$ into (28), the vector irrotational velocity potential A_θ is derived. Then, with ϕ, A_θ, B_2, by (24), (25), and (31), irrotational velocities u_n and u_t, and rotational velocity U_n are calculated respectively. Finally, by (30), (32) and (33), the next time-step position r, z, vector velocity potential B_2 and velocity potential ϕ are derived with the fourth-order Runge–Kutta method.

Repeating this procedure, we can simulate the drop oscillation. Because the drop is always symmetric about the z-axis as in figure 1, only half of the contour of the drop is simulated. In the program, 65 points from the top to the bottom along the grid line are used. To make the grids evenly spaced along the contour line, the grids are remeshed after every time iteration. In addition, the surface shape and the rotational and irrotational velocity potential are smoothed with the five-point numerical smoothing method (Longuet-Higgins & Cokelet 1976) in order to prevent high-frequency surface oscillations. In the calculation, the non-dimensional time step is 6.25×10^{-4}. Throughout the simulation, the volume of the drop changes by less

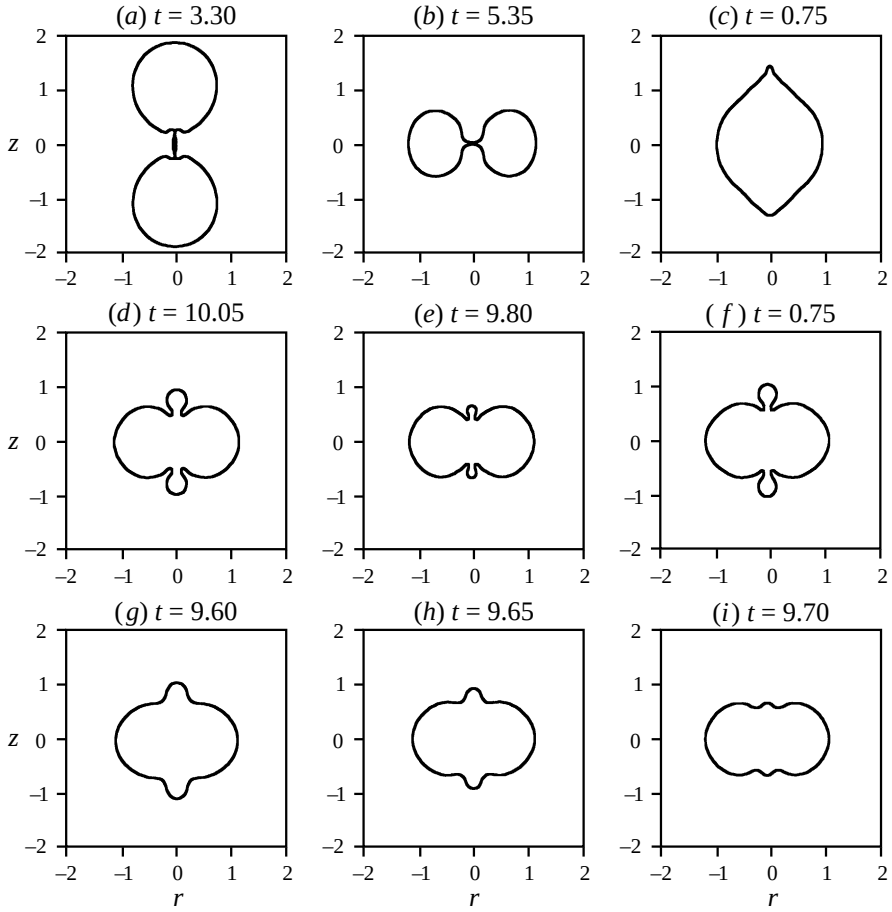

FIGURE 2. Different cases when calculation stops. (*a*) $Re = \infty$, $k^s = 0$ sP, $\mu^s = 0$ sP. (*b*) $Re = 892$, $k^s = 0$ sP, $\mu^s = 0$ sP. (*c*) $Re = 892$, $k^s = 0.050$ sP, $\mu_s = 0.001$ sP. (*d*) $Re = 892$, $k^s = 0.015$ sP, $\mu^s = 0.0005$ sP. (*e*) $Re = 892$, $k^s = 0.015$ sP, $\mu^s = 0.010$ sP. (*f*) $Re = 892$, $k^s = 0.015$ sP, $\mu^s = 0.015$ sP. A desired case: (*g–i*) $Re = 892$, $k^s = 0.020$ sP, $\mu^s = 0.010$ sP.

than 1% from its initial value. It is about 0.24% of its initial non-dimensional volume 4.188.

5. Analysis of results

With an excellent data set from space shuttle experiments (STS 73, Oct.-Nov., 1995) as a basis of comparison, we simulated the oscillations of a water drop with the surfactant Triton X-100. The initial deformed-drop parameters are as follows.

volume: 7.33 cm^3, equivalent spheric diameter: 2.41 cm
aspect ratio: 3.425
Triton concentration: 1.4×10^{-4} g ml^{-1} (1CMC)
the drop positions, r and z: from the image of the drop
surface tension σ (Apfel *et al.* 1997; Stebe 1989; Lin *et al.* 1990): 33 dyne cm^{-1}
drop density ρ: 1.0 g cm^{-3}
shear viscosity of the bulk phase μ : 0.01 cm^2 s^{-1}
from equation (19), we get a Reynolds number Re: 892
initial velocity potential ϕ and vector velocity potential B_2: 0.

In an earlier assessment of the first cycle of oscillation, Apfel *et al.* (1997) assumed zero surface viscosities and compensated for the additional damping by assuming a decreased Reynolds number. The best fit for surface tension in this circumstance was 33.0 dyne cm^{-1}, which is close to the values at the critical micelle concentration as measured by Stebe (1989) and by Lin *et al.* (1990). This initial estimate is shown in the present work to fit the data well over nine cycles of oscillations.

In equations (32) and (33), there are two unknown variables: surface dilatational viscosity k^s and surface shear viscosity μ^s. Our goal is to find the approximate k^s and μ^s so that simulations match experimentally observed oscillations. To do so, we calculate the case with both of them zero and take this result as a reference. With the knowledge that surface shear viscosity is smaller than surface dilatational viscosity (Edwards *et al.* 1991; Tian 1994), we keep μ^s small, 1.0×10^{-4} sP (surface poise), and increase the dilatational surface viscosity from 1.0×10^{-4} sP to 0.5 sP. Comparing the numerically simulated drop shapes with the experimental results, we analyse the damping constant and adjust k^s. Then in the same way, we choose μ^s. Finally, we find an optimal pair of k^s and μ^s. The result of the procedure yields surface dilatational and shear viscosities of 0.020 sP and 0.010 sP, respectively. Not only do these parameters rationalize the damping behaviours, but the detailed shapes of the greatly deformed drop match well with the observations.

To illustrate the sensitivity of the results to the choice of parameters, we provide the following examples:

1. Assume there is zero viscosity, with $\mu = k^s = \mu^s = 0$, in the oscillation of a drop. The simulation result in figure 2(*a*) shows that at time $t = 3.30$, the middle points of the left and right sides of the drop touch. The calculation is, therefore, terminated.

2. Consider only the shear viscosity of the bulk phase, with both of the surface viscosities zero. The simulation result in figure 2(*b*) shows that at time $t = 5.35$, almost at the end of the first cycle, the middle points of the top and bottom of the drop touch because of the small damping. The calculation stops.

3. In figure 2(*c*), $Re = 892$, $k^s = 0.050$ sP, $\mu^s = 0.001$ sP, with high surface dilatational viscosity, the drop deforms in a way that is completely different from the experimental observations in figure 3.

4. We consider both the surface viscosities and the shear viscosity of the bulk. In figure 2(*d*), 2(*e*) and 2(*f*), k^s is the same, 0.015 sP, with different μ^s, 0.005 sP, 0.010 sP and 0.015 sP respectively. Because the edges of the projected lobes at the top and bottom will touch, the calculation stops. Comparing these three cases, we find that the lobes in (*d*) and (*f*) are large and contract at the edges of the lobes. The lobes in (*f*) are thinner than those in (*d*). In (*e*), we see that the lobes are small and that the left and right sides of the lobes are almost parallel. If we adjust the surface viscosities so that the two sides of the lobes stretch towards the outside, then this case corresponds more closely to the situation of the real drop oscillation.

5. Compared with the experiment in figure 3, the shapes in figure 2(*g–i*) with the same Reynolds number, and same surface dilatational and shear viscosities, at non-dimensional time 9.60, 9.65, 9.70, respectively, are as desired. The two sides of the lobes at the centres of the top and bottom of the drop stretch toward the outside.

In the above five cases, we adjust the surface dilatational and shear viscosities by considering the drop shape at the time when the calculation terminates. In the calculation we also adjust them by comparing the oscillation shapes at other times with the corresponding experimental images in figure 3.

Shown in figure 3(*a–d*) are the first nine cycles of the drop oscillations with both experimental observations and numerical simulations. The analysis procedure for the

(*a*)

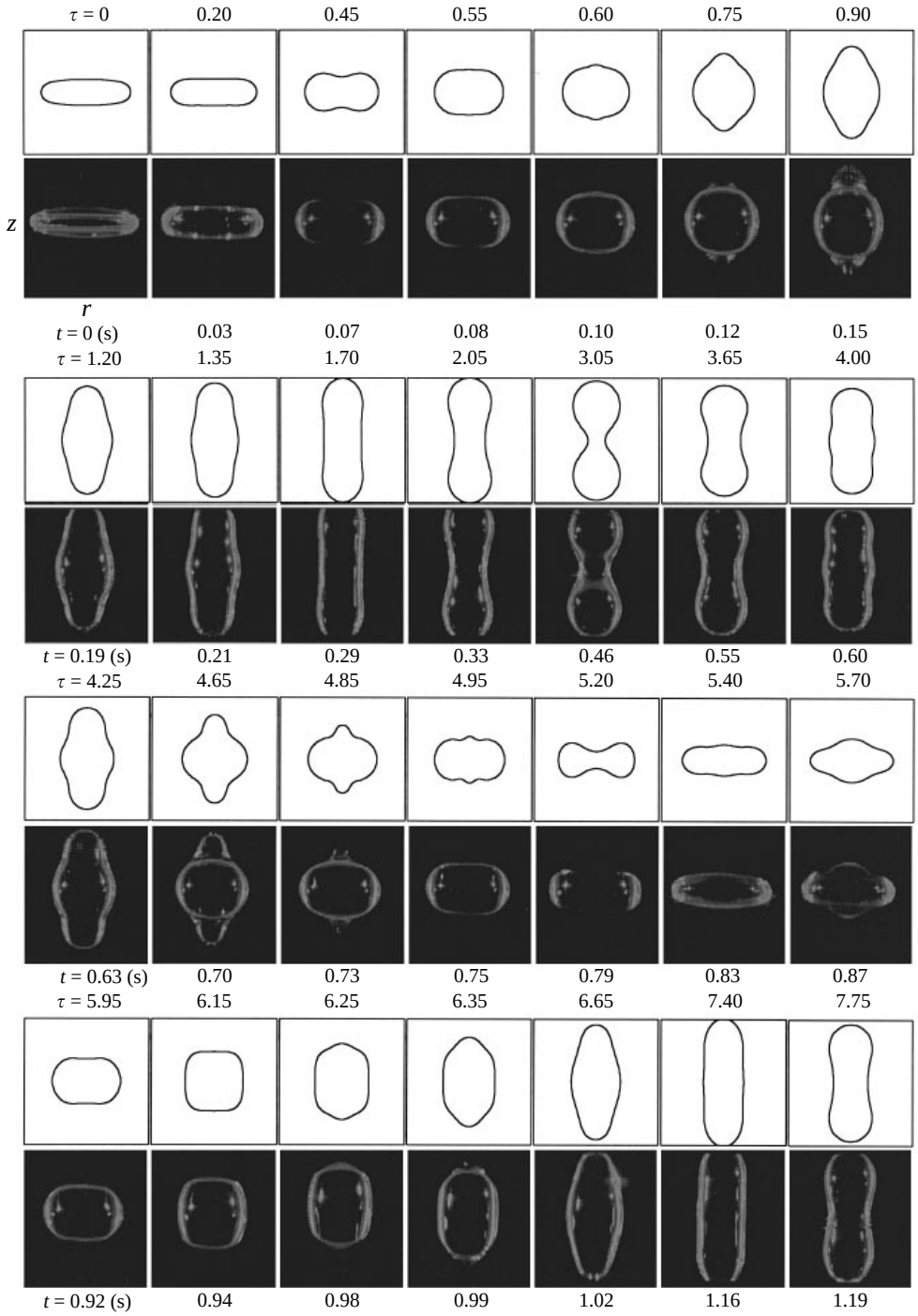

FIGURE 3(*a*). For caption see page 217.

(*b*)

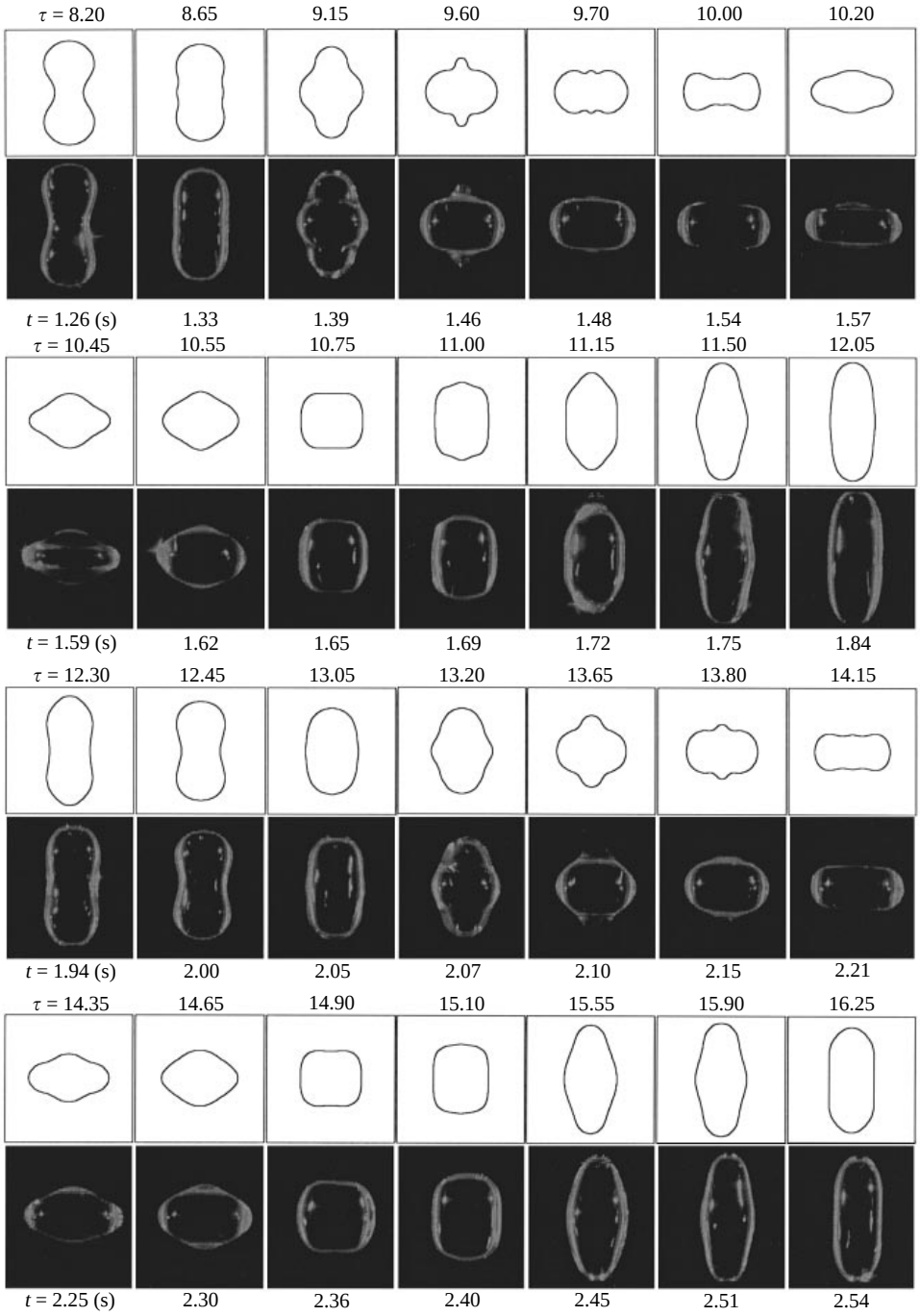

FIGURE 3(*b*). For caption see page 217.

(*c*)

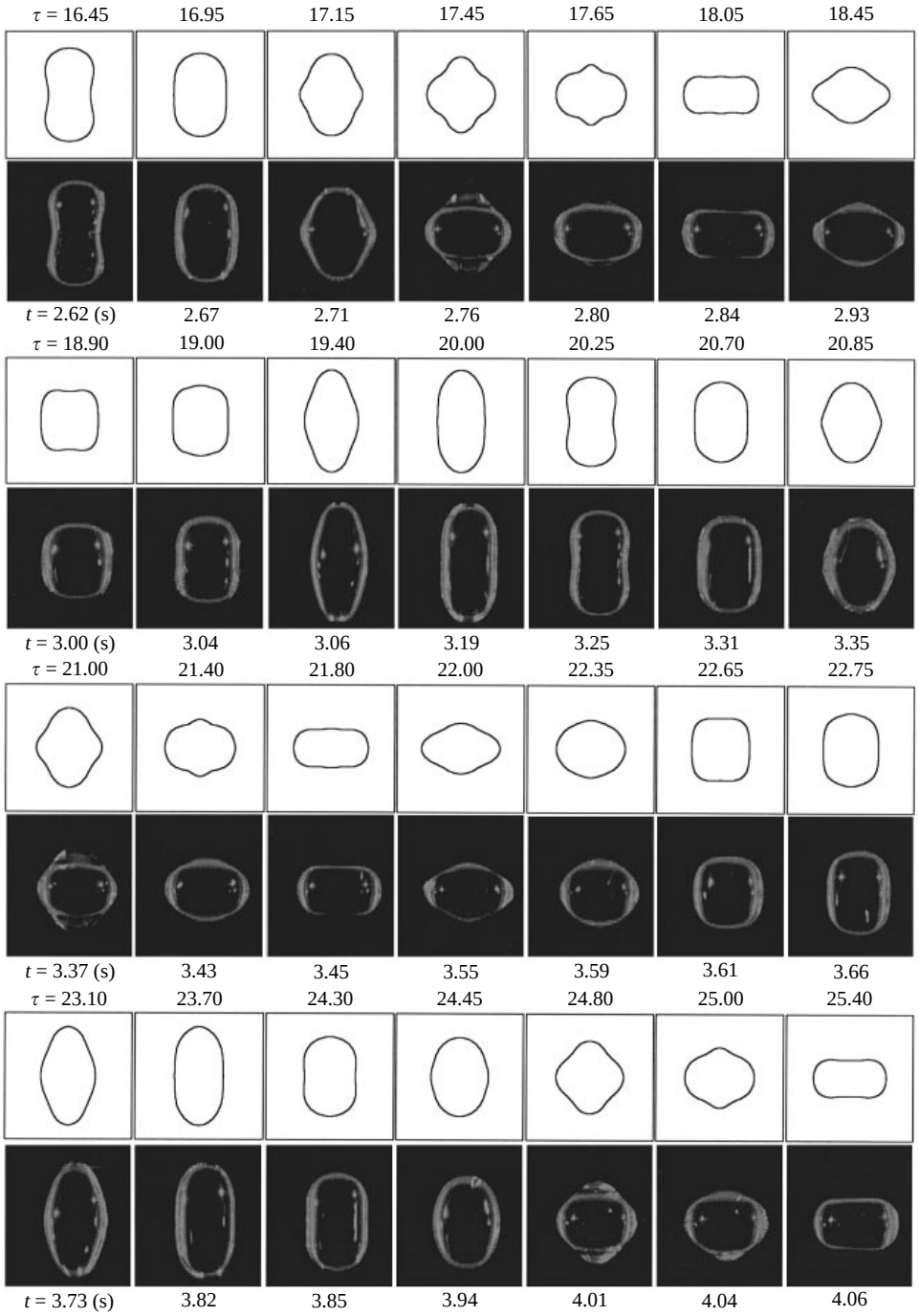

FIGURE 3(*c*). For caption see facing page.

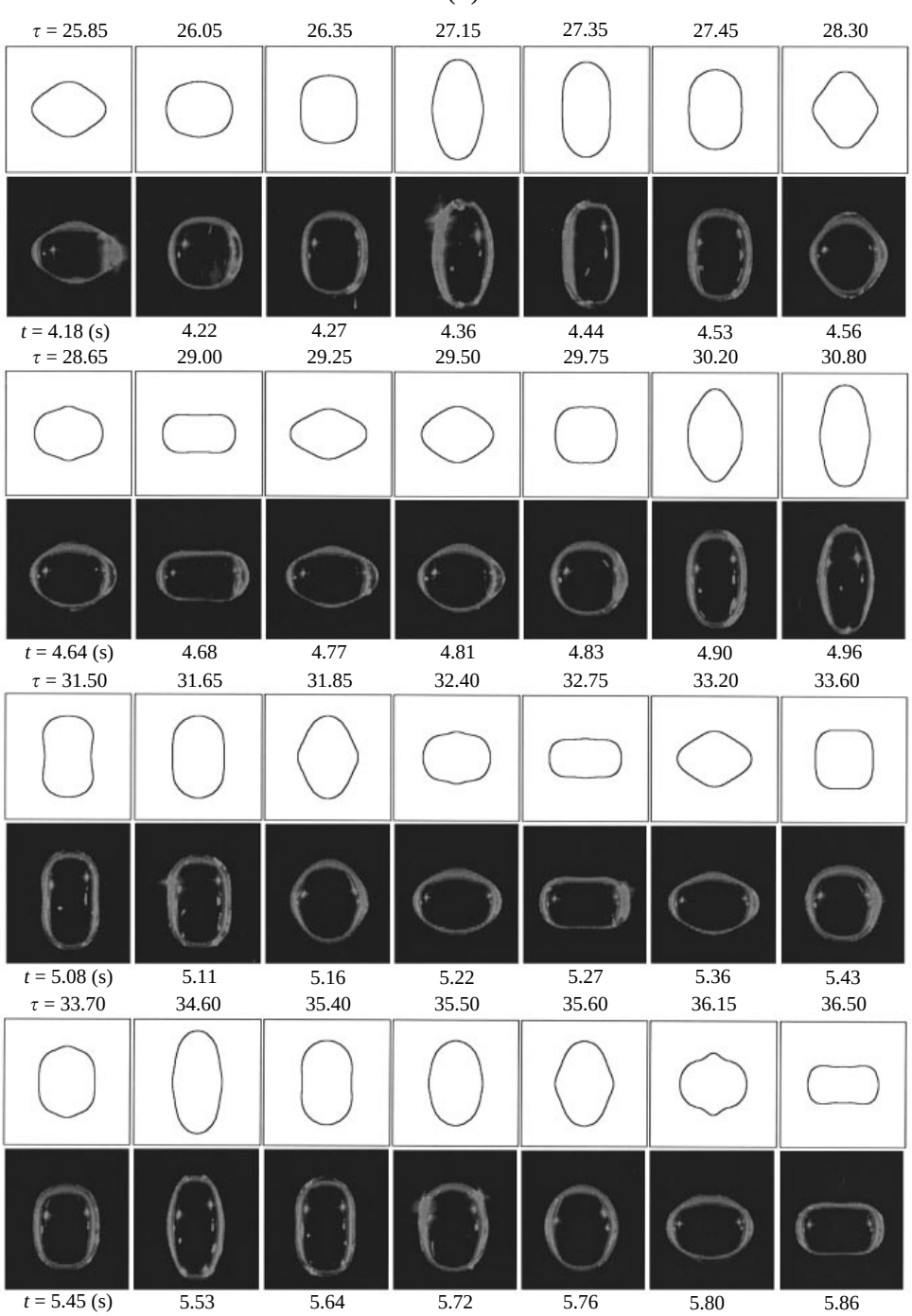

FIGURE 3(*d*). Experimental observations of nine complete cycles of superoscillation of a water drop (7.33 cm^3) with the surfactant Triton X-100 at the critical micelle concentration. The time in seconds is shown. Also shown (above) is the numerical simulation using the boundary-integral method. The time shown with the simulation is non-dimensional. (*a*) The first and part of the second cycles of oscillation; (*b*) the second to part of the fourth cycle of oscillation; (*c*) the fourth to the sixth cycle of oscillation; (*d*) the seventh to the ninth cycle of oscillation.

Cycle n	t(s) exp.	t_n/t_1	t sim.	t_n/t_1
1	0.85	1.0	5.35	1.0
2	0.72	1.1806	4.65	1.1505
3	0.70	1.2143	4.10	1.3049
4	0.66	1.2879	3.90	1.3718
5	0.63	1.3492	3.85	1.3896
6	0.62	1.3710	3.80	1.407
7	0.61	1.3934	3.75	1.4267
8	0.60	1.4167	3.70	1.4459
9	0.59	1.4407	3.70	1.4459
10	0.59	1.4407	3.70	1.4459

TABLE 1. Comparison of the time cycles of experiment and simulation.

drop oscillations in every cycle is almost the same. We use the cylindrical coordinate system in figure 1 to describe the first cycle of oscillation. A few points of comparison are noteworthy:

At the beginning, the left and right ends move toward the z-axis. The top and bottom move away from r-axis slowly. We can see the indentation at the top and bottom of the drop at numerical time 0.45. In the corresponding experimental image, we find that the outlines of the image at top and bottom are dim because the drop is concave in this region.

As we approach non-dimensional time 3.05, the oscillations show that the top and bottom of the drop stretch out, and the left and right ends move toward the z-axis.

Between the time 3.05 and 5.20, the left and right ends move away from the z-axis, the top and bottom move toward the r-axis. Because of inertia, at time 5.20 the top and bottom of the drop are indented again, and we can observe that those parts of the image are correspondingly dim.

If we compare the same shapes of the drop in different cycles, we can see that the width along the r-axis becomes wider and the length along the z-axis becomes shorter due to damping. The deformation also becomes smaller and the shape tends toward a sphere as the drop oscillates.

Comparing the shapes of the experimental images and the results of the numerical simulation over nine cycles, we observe that they match remarkably well. The ratio of the real experimental dimensional time below the images to the non-dimensional time above the simulated pictures in figure 3 is approximately 0.16 s. The numerical ratio of the time a_0/v_0 is 0.163 s. They also fit well. In addition, comparing the ratio of the time cycles of the experiment with that of the simulation, as in table 1, there is excellent correspondence.

With the simulation method, the surface shear viscosity and surface dilatational viscosity of the water drop with 1CMC Triton are found as 0.010 sP and 0.020 sP respectively. For a surfactant soluble in water, it is difficult to measure its surface dilatational viscosity experimentally, because the unknown diffusion rate from the bulk to the sublayer and the unknown sorption rate between the sublayer and the surface need to be considered. So far, we have not found any published experimental results for the two surface viscosities of Triton. We cannot judge the accuracy of the two surface viscosities derived through the simulation. However, it is well known that the surface shear viscosities of the water-soluble surfactants are in the range 10^{-3} sP to 10^{-1} sP. Our result is within this range. Furthermore, the surface viscosity

constants K_e and U_e are of the same order as the Reynolds number Re, in agreement with the experimental observations and the fitting analysis as described in §4.

6. Conclusion

Comparing numerical results with experimental results, we achieve good agreement when a unique pair of surface viscosity coefficients are chosen. The assumption that the surface tension remains constant and homogenous at the surface is useful for this special case. For a Reynolds number of 892, surface dilatational viscosity of 0.020 sP, and surface shear viscosity of 0.010 sP, we are able to take advantage of the boundary integral method to simulate this large deformation (beginning aspect ratio 3.425) and large-amplitude drop oscillation. In addition, we note that both surface dilatational viscosity and surface shear viscosity play a major role in the drop oscillation. We have provided a theoretical procedure that permits us to extract these properties by comparing experimental observations with numerical simulations of the drop oscillation.

The authors are indebted to Professor B. T. Chu for his instruction and guidance. We also thank the reviewers and editor for their helpful suggestions. This work is supported by NASA through JPL, contract 958722.

REFERENCES

Abramowitz, M. & Stegun, I. A. 1972 *Handbook of Mathematical Functions*. Washington, DC: Government Printing Office.

Alpert, B. K. 1990 Sparse representation of smooth linear operators. *Research rep*. Yale University.

Apfel, R. E., Tian, Y., Jankovsky, J., Shi, T. & Chen, X. 1997 Free oscillations and surfactant studies of superdeformed drops in microgravity. *Phys. Rev. Lett*. **78**, 1912–1915.

Batchelor, G. K. 1967 *An Introduction to Fluid Dynamics*. Cambridge University Press.

Boussinesq, M. J. 1913 The application of the formula for surface viscosity to the surface of a slowly falling droplet in the midst of a large unlimited amount of fluid which is at rest and possesses a smaller specific gravity. *Ann. Chim. Phys*. **29**, 357.

Edwards, D. A., Brenner, H. & Wasan, D. T. 1991 *Interfacial Transport Processes and Rheology*. Butterworth-Heinemann.

Holt, R. G., Tian, Y., Jankovsky, J. & Apfel, R. E. 1997 Surface-controlled drop oscillations in space. *J Acoust. Soc. Am*. **102**, 3802–3805.

Lamb, H. 1932 *Hydrodynamics*, 6th edn. Cambridge University Press.

Lin, S., Mckeigue, K. & Maldarelli, C. 1990 Diffusion-controlled surfactant adsorption studied by pendant drop digitization. *AICHE J*. **36**, 1785–1795.

Longuet-Higgins, M. S. & Cokelet, E. D. 1976 The deformation of steep surface wave on water I. Anumerical method of compution. *Proc. R. Soc. Lond*. A **350**, 1–26.

Lu, H. & Apfel, R. E. 1991 Shape oscillations of drops in the presence of surfactants. *J. Fluid Mech*. **222**, 351–368.

Lundgren, T. S. & Mansour, N. N. 1988 Oscillation of drops in zero gravity with weak viscous effects. *J. Fluid Mech*. **194**, 479–510.

Marangoni, C. G. M. 1871 Uber die ausbreitung der tropfen einer flussigkeit auf der oberfluche einer anderen. *Ann. Phys. (Poggendorff)* **3**, 337–354.

Scriven, L. E. 1960 Dynamics of a fluid interface. *Chem. Engng Sci*. **12**, 98–108.

Scriven, L. E. & Sternling, C. V. 1964 On cellular convection driven by surface-tension gradients: effect of mean surface tension and surface viscosity. *J. Fluid Mech*. **19**, 321–340.

Shi, T. & Apfel, R. E. 1995 Oscillation of a deformed liquid in an acoustic field. *Phys. Fluids* **7**, 1545–1551.

Shi, W. T., Apfel, R. E. & Holt, R. G. 1995 Instability of a deformed liquid drop in an acoustic field. *Phys. Fluids* **7**, 2601–2607.

Stebe, K. J. 1989 The remobilization of the interfaces of moving bubbles and droplets retarded by surfactant adsorption. PhD thesis, City University of New York.

Sternling, C. G. & Scriven, L. E. 1959 Interfacial turbulence: Hydrodynamic instability and the Marangoni effect. *AICHE J.* **5**, 514–523.

Tian, Y. 1994 Acoustic levitation and its applications in the study of liquid surface rheology. PhD thesis, Yale University.

Van Hunsel, J., Bleys, G. & Joos, P. 1986 Adsorption kinetics at the oil/water interface. *J. Colloid Interface Sci.* **114**, 432–441.